Numerical Simulation of the Molten-Pool Formation during the Laser Surface-Melting Process

KUNIMASA TAKESHITA and AKIRA MATSUNAWA

The boundary-fixing method, by which the moving-boundary problem is reduced into the fixed-boundary problem, has been applied to the numerical simulation of the molten-pool formation during the laser surface-melting process. A mathematical formulation and corresponding calculation scheme are developed for a model based on transient three-dimensional heat conduction with a moving solid-liquid interface. By the use of the boundary-fixing method, the heat balance at the solid-liquid interface is rigorously treated in the present numerical simulation. When the steady state is reached, the resulting molten pool is obtained without undulation in shape. The calculated results, based on an Al-32.7 wt pct Cu eutectic alloy, are discussed and compared with experimental data.

I. INTRODUCTION

LASER surface melting is of great interest in several technical applications because of its ability to improve mechanical or chemical properties of very localized surface regions and its possibilities for control and automation.[1] During laser surface melting of alloys, their surface regions remelt and rapidly solidify, resulting in the extension of solid-solubility limits, refinement of the scale of a microstructure, and the appearance of nonequilibrium phases.[2,3,4] In the case of this rapid solidification process, the rate of solidification mainly governs the possible appearance of nonequilibrium phases, their composition, and the scale of the microstructure.[4,5] Furthermore, the rate of solidification in this process can be determined quantitatively from the shape of the molten pool formed on the surface region of a substrate by irradiation of a moving high-power, high-density laser beam.[2] Therefore, in order to control the composition, the scale of the microstructure, and the extent of the laser-treated surface region, it is crucial to control the shape of the molten pool. Hence, numerical simulation based on a mathematical model of this process is of considerable importance to control the shape of the molten pool.

The shape of the molten pool is determined by the position of the solid-liquid interface within a substrate. Therefore, the problem of obtaining the shape of the molten pool is equivalent to that of finding the solid-liquid interface. This problem is mathematically categorized as the multidimensional moving-boundary problem, which is characterized by having a moving interface dividing the relevant field into two regions. The principal difficulty in the analysis of the multidimensional moving-boundary problems derives from the fact that the position of the moving boundary is not known *a priori* and that its shape is multidimensional.

In order to overcome this difficulty, the enthalpy method has been developed.[6–10] In this method, the enthalpy is used as a dependent variable along with the temperature in order that the latent heat due to phase change can be regarded as the heat capacity; thus, the moving interface is eliminated from consideration in the calculations. Because of its aforementioned advantage, the enthalpy method has been applied to several numerical simulations of the laser surface-melting process.[11,12,13] However, spatial oscillation of the numerical solution occurred, and, accordingly, the undulatory shape of the molten pool was simulated in the case of a substrate with a discrete phase-change temperature.[13]

Another technique used for solving the multidimensional moving-boundary problems is the boundary-fixing method.[14,15] This method includes an immobilization transformation and a numerical scheme for the solution of the transformed equations. Thereby, the moving-boundary problem is reduced into the fixed-boundary problem. Although the boundary-fixing method has its advantage for rigorously determining the position of the moving boundary, it has not yet been applied to the numerical simulation of the laser surface-melting process.

In this article, we apply the boundary-fixing method to the numerical simulation of the laser surface-melting process and demonstrate that the undulatory shape of the molten pool can be attained. The calculated results are compared with the experimental results performed using an Al-32.7 wt pct Cu eutectic alloy.[2]

II. MATHEMATICAL FORMULATION

A. *Model*

Figure 1 is a schematic drawing of the laser surface melting, showing a region of interest. A laser beam with a given beam radius (a) moves at a constant velocity (U). The axis of the laser beam is perpendicular to the upper surface of a semi-infinite substrate. The substrate surface is irradiated with the laser beam, and a molten pool surrounded by a heat-affected region is formed due to the energy transfer between the laser beam and the substrate surface. The molten pool moves with the laser beam, resulting in the formation of a solidified trace behind it. A Cartesian and a spherical coordinate system move with the laser beam at the same velocity. The origins of these coordinate systems, denoted by the letter O in Figure 1, coincide with each other. In order to rapidly obtain converged solutions of the present problem, the origin is set apart behind the center of the laser

KUNIMASA TAKESHITA, Associate Professor, is with the Department of Mechanical Engineering, Faculty of Engineering, Fukui University, Fukui 910-8507, Japan. AKIRA MATSUNAWA, Professor, is with the Joining and Welding Research Institute, Osaka University, Osaka 567-0047, Japan.

Manuscript submitted November 6, 2000.

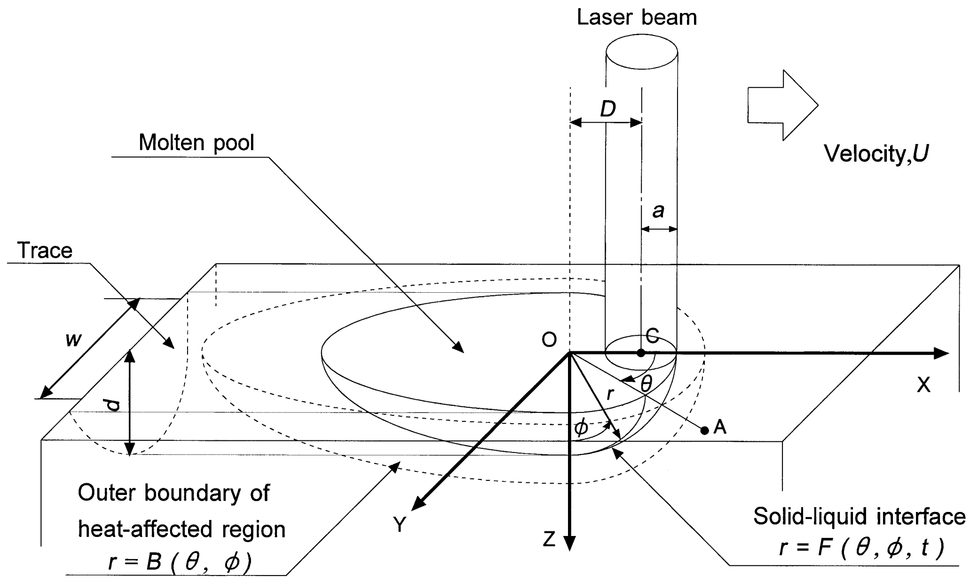

Fig. 1—Schematic drawing of laser surface melting showing a region of interest.

beam, denoted by C in Figure 1, by a distance of D. The procedure to determine the value of D is explained in Section III.A. In the Cartesian coordinate system, the x-direction is parallel to the movement of the laser beam, the z-direction is into the substrate, and the y-direction is the third orthogonal axis, as shown in Figure 1. The boundary between the molten pool and the heat-affected region is the solid-liquid interface, represented by the function $F(\theta, \phi, t)$ in the spherical coordinate system (r, θ, ϕ). The outer boundary of the heat-affected region is the isothermal surface within the substrate, the temperature over which is set at an arbitrary temperature (T_B) close to the initial temperature of the substrate (T_i), and its function is represented by $B(\theta, \phi)$ in the spherical coordinate system.

If it is assumed that a quasi–steady state is established, there exists a steady molten pool which does not change with time. The problem then is to find the profile of this molten pool and the distributions of temperature in the molten pool and the adjacent heat-affected region. In formulating the model, some further assumptions and simplifications are introduced to the problem. They are as follows

(1) Convective heat transfer in the molten pool is ignored.
(2) Radiation heat loss from the upper surface of the substrate is considered.
(3) Convective heat loss from the upper surface of the substrate due to shielding gas flow is considered.
(4) The temperature on the upper surface of the molten pool does not exceed the vaporization temperature of the substrate.
(5) The substrate melts and solidifies at a single temperature with a planar solid-liquid interface.
(6) The substrate thermal conductivity, specific heat, thermal diffusivity, and surface absorptivity are temperature independent.
(7) The power distribution in the laser beam is Gaussian.

B. *Governing Equations*

Assumptions 1 and 5 allow this problem to be treated as a three-dimensional heat-conduction problem with a moving planar solid-liquid interface. Referring to Figure 1 and the terms defined in the Nomenclature, the governing equations for the molten pool (liquid region) and the heat-affected region (solid region) will be described in the moving spherical coordinate as follows.

The basic heat-flow equation within the liquid region is

$$\frac{\partial T_L}{\partial t} - U\left(\sin\phi\cos\theta\frac{\partial T_L}{\partial r} - \frac{\sin\theta}{r\sin\phi}\frac{\partial T_L}{\partial\theta} + \frac{\cos\theta\cos\phi}{r}\frac{\partial T_L}{\partial\phi}\right) = \alpha_L\left(\frac{\partial^2 T_L}{\partial r^2} + \frac{2}{r}\frac{\partial T_L}{\partial r} + \frac{1}{r^2}\frac{\partial^2 T_L}{\partial\phi^2} + \frac{\cot\phi}{r^2}\frac{\partial T_L}{\partial\phi} + \frac{1}{r^2\sin^2\phi}\frac{\partial^2 T_L}{\partial\theta^2}\right) \qquad [1]$$

with the boundary conditions

$$T_L = T_f \quad \text{on} \quad r = F(\theta, \phi, t) \qquad [2]$$

$$\frac{K_L}{r}\frac{\partial T_L}{\partial\phi} = \beta_L q(r) - h(T_L - T_a) - \varepsilon_L\sigma(T_L^4 - T_a^4) \quad \text{on} \quad \phi = \pi/2 \quad \text{and} \quad 0 < r < F(\theta, \pi/2, t) \qquad [3]$$

and

$$-K_L\frac{\partial T_L}{\partial z} = \beta_L q(0) - h(T_L - T_a) - \varepsilon_L\sigma(T_L^4 - T_a^4) \quad \text{at} \quad x, y, z = 0 \qquad (i.e., r = 0) \qquad [4]$$

The boundary condition [3] cannot be adopted at $r = 0$, because its left-hand-side term becomes infinite when r approaches zero. Therefore, the singularity at $r = 0$ necessitates another boundary condition, Eq. [4], expressed in the moving Cartesian coordinate. For the convenience of formulation, the left-hand-side term of Eq. [4] can be rewritten in the moving spherical coordinate as

$$-K_L\lim_{r,\phi\to 0}\frac{\partial T_L}{\partial r} = \beta_L q(0) - h(T_L - T_a) - \varepsilon_L\sigma(T_L^4 - T_a^4) \qquad [5]$$

The basic heat-flow equation within the solid region is

$$\frac{\partial T_S}{\partial t} - U\left(\sin\phi\cos\theta\frac{\partial T_S}{\partial r} - \frac{\sin\theta}{r\sin\phi}\frac{\partial T_S}{\partial\theta} + \frac{\cos\theta\cos\phi}{r}\frac{\partial T_S}{\partial\phi}\right)$$
$$= \alpha_S\left(\frac{\partial^2 T_S}{\partial r^2} + \frac{2}{r}\frac{\partial T_S}{\partial r} + \frac{1}{r^2}\frac{\partial^2 T_S}{\partial\phi^2} + \frac{\cot\phi}{r^2}\frac{\partial T_S}{\partial\phi} + \frac{1}{r^2\sin^2\phi}\frac{\partial^2 T_S}{\partial\theta^2}\right) \quad [6]$$

with the boundary conditions

$$T_S = T_f \quad \text{on} \quad r = F(\theta,\phi,t) \quad [7]$$

$$\frac{K_S}{r}\frac{\partial T_S}{\partial\phi} = \beta_S q(r) - h(T_S - T_a) - \varepsilon_S\sigma(T_S^4 - T_a^4)$$
$$\text{on} \quad \phi = \pi/2 \quad \text{and} \quad F(\theta, \pi/2, t) < r < B(\theta, \pi/2) \quad [8]$$

and

$$T_S = T_B \quad \text{on} \quad r = B(\theta, \phi) \quad [9]$$

The value $q(r)$ in Eqs. [3], [5], and [8] is that given by a Gaussian power distribution as

$$q(r) = \frac{2P}{\pi a^2}\exp\left(-\frac{r^2 + D^2 - 2rD\cos\theta}{a^2}\right) \quad [10]$$

In Eq. [10], r is the distance from the origin O to an arbitrary point on the substrate surface, denoted by A in Figure 1, and θ is the angle between the x-axis and the line $\overline{OA}$. Thus, the value of $(r^2 + D^2 - 2rD\cos\theta)$ in Eq. [10] gives the square of the distance from the center of the laser beam to the point A.

The heat balance at the solid-liquid interface provides the following boundary conditions, given by

$$\frac{\partial F}{\partial t} + U\left(\sin\phi\cos\theta + \frac{\sin\theta}{F\sin\phi}\frac{\partial F}{\partial\theta} - \frac{\cos\phi\cos\theta}{F}\frac{\partial F}{\partial\phi}\right)$$
$$= \frac{1}{L}\left(-K_L\frac{\partial T_L}{\partial r} + K_S\frac{\partial T_S}{\partial r} + \frac{1}{F^2\sin^2\phi}\frac{\partial F}{\partial\theta}\left(K_L\frac{\partial T_L}{\partial\theta} - K_S\frac{\partial T_S}{\partial\theta}\right) + \frac{1}{F^2}\frac{\partial F}{\partial\phi}\left(K_L\frac{\partial T_L}{\partial\phi} - K_S\frac{\partial T_S}{\partial\phi}\right)\right) \quad [11]$$
$$\text{on} \quad r = F(\theta, \phi, t) \quad \text{and} \quad \phi \neq \pi/2$$

and

$$\frac{\partial F}{\partial t} + U\left(\cos\theta + \frac{\sin\theta}{F}\frac{\partial F}{\partial\theta}\right) = \frac{1}{L}\left(-K_L\frac{\partial T_L}{\partial r} + K_S\frac{\partial T_S}{\partial r} + \frac{1}{F^2}\frac{\partial F}{\partial\theta}\left(K_L\frac{\partial T_L}{\partial\theta} - K_S\frac{\partial T_S}{\partial\theta}\right) + \frac{1}{F^2}\frac{\partial F}{\partial\phi}\left(K_L\frac{\partial T_L}{\partial\phi} - K_S\frac{\partial T_S}{\partial\phi}\right) + \beta_o q(r) - h(T_f - T_a) - \varepsilon_o\sigma(T_f^4 - T_a^4)\right) \quad [12]$$
$$\text{on} \quad r = F(\theta, \pi/2, t)$$

C. *Boundary-Fixing Formulation*

The following two independent variables are introduced for the present problem:

for the liquid region,

$$\eta = \frac{r}{F(\theta, \phi, t)} \quad [13]$$

and for the solid region,

$$\xi = \frac{r - B(\theta, \phi)}{F(\theta, \phi, t) - B(\theta, \phi)} \quad [14]$$

The correspondence between the physical body and the transformed body is schematically represented in Figure 2. The liquid and solid regions are both transformed into semispheres with a unit radius. The spherical surfaces of the semispheres, *i.e.*, $\eta = 1$ and $\xi = 1$, correspond to the solid-liquid interface.

The resultant governing equation for the liquid region is described as

$$\frac{\partial T_L}{\partial t} = \left(\frac{\alpha_L}{\eta^2F^2\sin^2\phi}\left(\frac{\partial\eta}{\partial\theta}\right)^2 + \frac{\alpha_L}{\eta^2F^2}\left(\frac{\partial\eta}{\partial\phi}\right)^2 + \frac{\alpha_L}{F^2}\right)\frac{\partial^2 T_L}{\partial\eta^2}$$
$$+ \left(\frac{\alpha_L}{\eta^2F^2\sin^2\phi}\frac{\partial^2\eta}{\partial\theta^2} + \frac{\alpha_L}{\eta^2F^2}\frac{\partial^2\eta}{\partial\phi^2} - \frac{U\sin\theta}{\eta F\sin\phi}\frac{\partial\eta}{\partial\theta}\right.$$
$$+ \left(\frac{\alpha_L\cot\phi}{\eta^2F^2} + \frac{U\cos\phi\cos\theta}{\eta F}\right)\frac{\partial\eta}{\partial\phi} + \frac{2\alpha_L}{\eta F^2} \quad [15]$$
$$\left. + \frac{U\sin\phi\cos\theta}{F} - \frac{\partial\eta}{\partial t}\right)\frac{\partial T_L}{\partial\eta} + \frac{2\alpha_L}{\eta^2F^2\sin^2\phi}\frac{\partial\eta}{\partial\theta}\frac{\partial^2 T_L}{\partial\eta\partial\theta}$$
$$+ \frac{2\alpha_L}{\eta^2F^2}\frac{\partial\eta}{\partial\phi}\frac{\partial^2 T_L}{\partial\eta\partial\phi} + \frac{\alpha_L}{\eta^2F^2\sin^2\phi}\frac{\partial^2 T_L}{\partial\theta^2} + \frac{\alpha_L}{\eta^2F^2}\frac{\partial^2 T_L}{\partial\phi^2}$$
$$- \frac{U\sin\theta}{\eta F\sin\phi}\frac{\partial T_L}{\partial\theta} + \left(\frac{\alpha_L\cot\phi}{\eta^2F^2} + \frac{U\cos\phi\cos\theta}{\eta F}\right)\frac{\partial T_L}{\partial\phi}$$

With the boundary conditions

$$T_L = T_f \quad \text{on} \quad \eta = 1 \quad [16]$$

$$\frac{K_L}{\eta F}\left(\frac{\partial T_L}{\partial\phi} - \frac{\eta}{F}\frac{\partial F}{\partial\phi}\frac{\partial T_L}{\partial\eta}\right) = \beta_L q(\eta F) - h(T_L - T_a)$$
$$- \varepsilon_L\sigma(T_L^4 - T_a^4) \quad \text{on} \quad \phi = \pi/2 \quad \text{and} \quad 0 < \eta < 1 \quad [17]$$

and

$$-K_L\lim_{\eta,\phi\to 0}\frac{1}{F}\frac{\partial T_L}{\partial\eta} = \beta_L q(0) - h(T_L - T_a)$$
$$- \varepsilon_L\sigma(T_L^4 - T_a^4) \quad \text{at} \quad \eta = 0 \quad [18]$$

The transformed governing equation for the solid region is also described as

$$\frac{\partial T_S}{\partial t} = \left(\frac{\alpha_S}{(\xi(F - B) + B)^2\sin^2\phi}\left(\frac{\partial\xi}{\partial\theta}\right)^2 + \frac{\alpha_S}{(\xi(F - B) + B)^2}\left(\frac{\partial\xi}{\partial\phi}\right)^2 + \frac{\alpha_S}{(F - B)^2}\right)\frac{\partial^2 T_S}{\partial\xi^2}$$
$$+ \left(\frac{\alpha_S}{(\xi(F - B) + B)^2\sin^2\phi}\frac{\partial^2\xi}{\partial\theta^2}\right.$$
$$+ \frac{\alpha_S}{(\xi(F - B) + B)^2}\frac{\partial^2\xi}{\partial\phi^2}$$

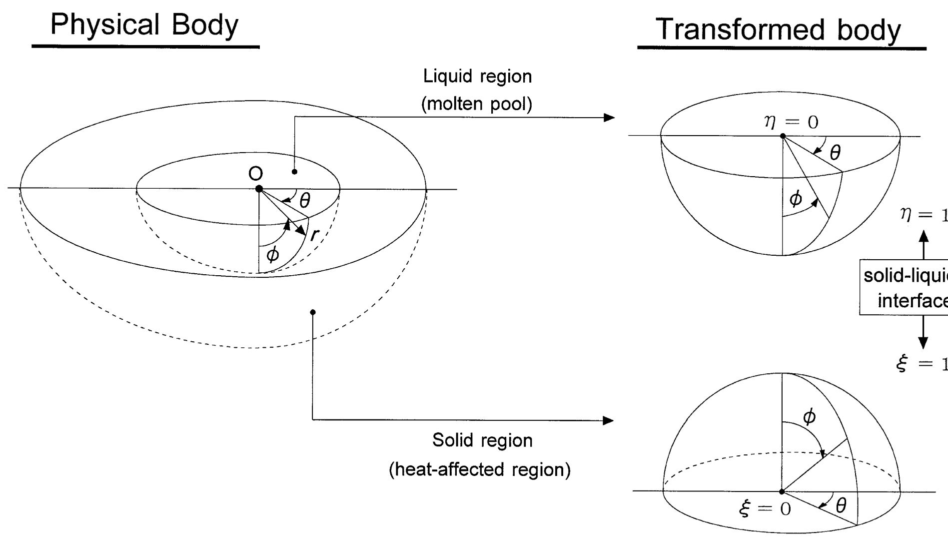

Fig. 2—Correspondence between physical and transformed bodies.

$$
\begin{aligned}
&- \frac{U \sin\theta}{(\xi(F-B)+B)\sin\phi}\frac{\partial\xi}{\partial\theta} \\
&+ \left(\frac{\alpha_S \cot\phi}{(\xi(F-B)+B)^2} + \frac{U\cos\phi\cos\theta}{\xi(F-B)+B}\right)\frac{\partial\xi}{\partial\phi} \\
&+ \frac{2\alpha_S}{(F-B)(\xi(F-B)+B)} + \frac{U\sin\phi\cos\theta}{F-B} \qquad [19] \\
&- \left.\frac{\partial\xi}{\partial t}\right)\frac{\partial T_S}{\partial\xi} + \frac{2\alpha_S}{(\xi(F-B)+B)^2\sin^2\phi}\frac{\partial\xi}{\partial\theta}\frac{\partial^2 T_S}{\partial\xi\partial\theta} \\
&+ \frac{2\alpha_S}{(\xi(F-B)+B)^2}\frac{\partial\xi}{\partial\phi}\frac{\partial^2 T_S}{\partial\xi\partial\phi} \\
&+ \frac{\alpha_S}{(\xi(F-B)+B)^2\sin^2\phi}\frac{\partial^2 T_S}{\partial\theta^2} \\
&+ \frac{\alpha_S}{(\xi(F-B)+B)^2}\frac{\partial^2 T_S}{\partial\phi^2} \\
&- \frac{U\sin\theta}{(\xi(F-B)+B)\sin\phi}\frac{\partial T_S}{\partial\theta} \\
&+ \left(\frac{\alpha_S\cot\phi}{(\xi(F-B)+B)^2} + \frac{U\cos\phi\cos\theta}{\xi(F-B)+B}\right)\frac{\partial T_S}{\partial\phi}
\end{aligned}
$$

with the boundary conditions

$$T_S = T_f \quad \text{on} \quad \xi = 1 \qquad [20]$$

$$
\begin{aligned}
&\frac{K_S}{\xi(F-B)+B}\left(\frac{\partial T_S}{\partial\phi} - \frac{1}{F-B}\left(\frac{\partial B}{\partial\phi} + \xi\left(\frac{\partial F}{\partial\phi} - \frac{\partial B}{\partial\phi}\right)\right)\frac{\partial T_S}{\partial\xi}\right) \\
&= \beta_S q(\xi(F-B)+B) - h(T_S - T_a) \qquad [21] \\
&- \varepsilon_S\sigma(T_S^4 - T_a^4) \quad \text{on} \quad \phi = \pi/2 \quad \text{and} \quad 0 < \xi < 1
\end{aligned}
$$

and

$$T_S = T_B \quad \text{at} \quad \xi = 0 \qquad [22]$$

In Eqs. [15] and [19], the derivatives $\partial\eta/\partial t$, $\partial\eta/\partial\phi$, $\partial^2\eta/\partial\phi^2$, $\partial\eta/\partial\theta$, $\partial^2\eta/\partial\theta^2$, $\partial\xi/\partial t$, $\partial\xi/\partial\phi$, $\partial^2\xi/\partial\phi^2$, $\partial\xi/\partial\theta$, and $\partial^2\xi/\partial\theta^2$ are given by

$$\frac{\partial\eta}{\partial t} = -\frac{\eta}{F}\frac{\partial F}{\partial t} \qquad [23]$$

$$\frac{\partial\eta}{\partial\phi} = -\frac{\eta}{F}\frac{\partial F}{\partial\phi} \qquad [24]$$

$$\frac{\partial^2\eta}{\partial\phi^2} = -\frac{1}{F}\left(\eta\frac{\partial^2 F}{\partial\phi^2} + 2\frac{\partial\eta}{\partial\phi}\frac{\partial F}{\partial\phi}\right) \qquad [25]$$

$$\frac{\partial\eta}{\partial\theta} = -\frac{\eta}{F}\frac{\partial F}{\partial\theta} \qquad [26]$$

$$\frac{\partial^2\eta}{\partial\theta^2} = -\frac{1}{F}\left(\eta\frac{\partial^2 F}{\partial\theta^2} + 2\frac{\partial\eta}{\partial\theta}\frac{\partial F}{\partial\theta}\right) \qquad [27]$$

$$\frac{\partial\xi}{\partial t} = -\frac{\xi}{F-B}\frac{\partial F}{\partial t} \qquad [28]$$

$$\frac{\partial\xi}{\partial\phi} = -\frac{1}{F-B}\left(\frac{\partial B}{\partial\phi} + \xi\left(\frac{\partial F}{\partial\phi} - \frac{\partial B}{\partial\phi}\right)\right) \qquad [29]$$

$$
\begin{aligned}
\frac{\partial^2\xi}{\partial\phi^2} = -\frac{1}{F-B}&\left(\frac{\partial^2 B}{\partial\phi^2} + 2\frac{\partial\xi}{\partial\phi}\left(\frac{\partial F}{\partial\phi} - \frac{\partial B}{\partial\phi}\right)\right. \\
&\left. + \xi\left(\frac{\partial^2 F}{\partial\phi^2} - \frac{\partial^2 B}{\partial\phi^2}\right)\right)
\end{aligned} \qquad [30]
$$

$$\frac{\partial\xi}{\partial\theta} = -\frac{1}{F-B}\left(\frac{\partial B}{\partial\theta} + \xi\left(\frac{\partial F}{\partial\theta} - \frac{\partial B}{\partial\theta}\right)\right) \qquad [31]$$

and

$$
\begin{aligned}
\frac{\partial^2\xi}{\partial\theta^2} = -\frac{1}{F-B}&\left(\frac{\partial^2 B}{\partial\theta^2} + 2\frac{\partial\xi}{\partial\theta}\left(\frac{\partial F}{\partial\theta} - \frac{\partial B}{\partial\theta}\right)\right. \\
&\left. + \xi\left(\frac{\partial^2 F}{\partial\theta^2} - \frac{\partial^2 B}{\partial\theta^2}\right)\right)
\end{aligned} \qquad [32]
$$

The heat-balance equations at the solid-liquid interface are transformed into

$$\frac{\partial F}{\partial t} + U\left(\sin\phi\cos\theta + \frac{\sin\theta}{F\sin\phi}\frac{\partial F}{\partial\theta} - \frac{\cos\phi\cos\theta}{F}\frac{\partial F}{\partial\phi}\right)$$
$$= \frac{1}{L}\left(1 + \frac{1}{F^2\sin^2\phi}\left(\frac{\partial F}{\partial\theta}\right)^2 + \frac{1}{F^2}\left(\frac{\partial F}{\partial\phi}\right)^2\right) \quad [33]$$
$$\cdot\left(-\frac{K_L}{F}\frac{\partial T_L}{\partial\eta} + \frac{K_S}{F-B}\frac{\partial T_S}{\partial\xi}\right) \quad \text{on} \quad \eta = \xi = 1$$
$$\text{and} \quad \phi \neq \pi/2$$

and

$$\frac{\partial F}{\partial t} + U\left(\cos\theta + \frac{\sin\theta}{F}\frac{\partial F}{\partial\theta}\right) = \frac{1}{L}\left(1 + \frac{1}{F^2}\left(\frac{\partial F}{\partial\theta}\right)^2\right.$$
$$\left. + \frac{1}{F^2}\left(\frac{\partial F}{\partial\phi}\right)^2\right)\cdot\left(-\frac{K_L}{F}\frac{\partial T_L}{\partial\eta} + \frac{K_S}{F-B}\frac{\partial T_S}{\partial\xi}\right) \quad [34]$$
$$+ \frac{1}{L}\left(\beta_o q(F) - h(T_f - T_a) - \varepsilon_o\sigma(T_f^4 - T_a^4)\right)$$
$$\text{on} \quad \eta = \xi = 1 \quad \text{and} \quad \phi = \pi/2$$

D. *Numerical Method of Solution*

The solution of the present problem was obtained as a steady-state ultimate solution of an artificial transient problem. The governing Eqs. [15] and [19], the boundary conditions [16] through [18] and [20] through [22], and the heat-balance Eqs. [33] and [34] were nondimensioned using the following variables:

$$T_L^* = \frac{T_L - T_f}{T_f - T_B}, \quad T_S^* = \frac{T_S - T_f}{T_f - T_B},$$
$$T_a^* = \frac{T_a - T_f}{T_f - T_B}, \quad t^* = \frac{\alpha_o t}{a^2},$$
$$\phi^* = \frac{\phi}{\phi_o}, \quad \theta^* = \frac{\theta}{\theta_o}, \quad r^* = \frac{r}{a}, \quad F^* = \frac{F}{a}, \quad B^* = \frac{B}{a}, \quad [35]$$
$$U^* = \frac{Ua}{\alpha_o}, \quad \alpha_L^* = \frac{\alpha_L}{\alpha_o}, \quad \alpha_S^* = \frac{\alpha_S}{\alpha_o}, \quad K_L^* = \frac{K_L}{K_o}, \quad K_S^* = \frac{K_S}{K_o},$$
$$L^* = \frac{\alpha_o L}{K_o(T_f - T_B)}, \quad h^* = \frac{ha}{K_o},$$
$$\sigma^* = \frac{\sigma a(T_f - T_B)^3}{K_o}, \quad \text{and} \quad P^* = \frac{P}{aK_o(T_f - T_B)}$$

The explicit finite-difference method was employed because of the simplicity of the calculation. Due to symmetry with respect to the center plane (*i.e.*, the $\theta = 0$ and π plane) of the semispherical liquid and solid regions shown in Figure 2, the temperature fields were calculated on only one side of the center plane. The numbers of nodal points within the regions considered were 10 in the η direction, 40 in the ξ direction, 8 in the ϕ direction, and 13 in the θ direction, respectively. Forward-difference approximation was used for time derivatives in Eqs. [15], [19], [33], and [34]. For the spatial derivatives $\partial T_L/\partial\eta$, $\partial T_L/\partial\theta$, and $\partial T_L/\partial\phi$ in Eq. [15], $\partial T_S/\partial\xi$, $\partial T_S/\partial\theta$, and $\partial T_S/\partial\phi$ in Eq. [19], and $\partial F/\partial\theta$ and $\partial F/\partial\phi$ in Eqs. [33] and [34], upstream-difference approximation was used because of its advantage in stability of calculation. Central- or backward-difference approximation was used for the other spatial derivatives in Eqs. [15], [19], [33], and [34]. The procedures for the calculation are as follows.

(1) The initial position of the solid-liquid interface $F(\theta, \phi, 0)$, the outer boundary position $B(\theta, \phi)$, and the initial temperature distributions $T_L(\eta, \theta, \phi, 0)$ and $T_S(\xi, \theta, \phi, 0)$ in both the liquid and solid regions are set using the analytical solution of the Rosenthal moving-point source model.[16]
(2) The new position of the solid-liquid interface $F(\theta, \phi, t)$ and the new temperature distributions $T_L(\eta, \theta, \phi, t)$ and $T_S(\xi, \theta, \phi, t)$ in both the regions are calculated from the explicit approximation of Eqs. [15], [19], [33], and [34] using the Euler method[17] with respect to time.
(3) The new temperature distributions $T_L(\eta, \theta, \pi/2, t)$ and $T_S(\xi, \theta, \pi/2, t)$ on the upper surfaces of the liquid and solid regions are calculated from the backward-difference approximation of Eqs. [17], [18], and [21] using $F(\theta, \phi, t)$, $T_L(\eta, \theta, \phi, t)$, and $T_S(\xi, \theta, \phi, t)$ at a new time level. If the obtained temperature $T_L(\eta, \theta, \pi/2, t)$ at a nodal point on the upper surface of the liquid region exceeds the vaporization temperature of the substrate (T_V), then the temperature at the nodal point is set equal to the vaporization temperature of the substrate, in accordance with assumption 4.
(4) The maximum value of $\partial F^*/\partial t^*$ (equal to $(a/\alpha_o)\partial F/\partial t$) at a new time level is obtained using Eqs. [33] and [34] and then is checked if it is within the given value of 10^{-6} to judge whether the steady state is reached.
(5) If the steady state is not reached, the same procedures 2 and 3 are repeated.

To avoid a numerical instability, the stability condition given by the inequality (Eq. [36]) was considered on determining a time step for calculation (Δt) with respect to the chosen spatial increments $\Delta\eta$, $\Delta\xi$, $\Delta\theta$, and $\Delta\phi$:

$$\Delta t \leq \min\,(\Delta t_L, \Delta t_S, \Delta t_F) \quad [36]$$

In Eq. [36], Δt_L can be derived from Eq. [15], Δt_S from Eq. [19], and Δt_F from Eqs. [33] and [34] as[18]

$$\Delta t_L = \min\left(\left(\left(\frac{1}{\eta_i^2 F_{k,l}^2\sin^2\phi_l}\left(\frac{\partial\eta}{\partial\theta}\right)^2_{i,k,l} + \frac{1}{\eta_i^2 F_{k,l}^2}\left(\frac{\partial\eta}{\partial\phi}\right)^2_{i,k,l}\right.\right.\right.$$
$$\left. + \frac{1}{F_{k,l}^2}\right)\cdot\frac{2\alpha_L}{(\Delta\eta)^2} + \frac{2\alpha_L}{\eta_i^2 F_{k,l}^2\sin^2\phi_l\cdot(\Delta\theta)^2} + \frac{2\alpha_L}{\eta_i^2 F_{k,l}^2(\Delta\phi)^2}$$
$$+ \frac{4\alpha_L}{\eta_i^2 F_{k,l}^2\sin^2\phi_l\cdot(\Delta\eta\Delta\theta)}\cdot\left|\left(\frac{\partial\eta}{\partial\theta}\right)_{i,k,l}\right| + \frac{4\alpha_L}{\eta_i^2 F_{k,l}^2(\Delta\eta\Delta\phi)}$$
$$\cdot\left|\left(\frac{\partial\eta}{\partial\phi}\right)_{i,k,l}\right| + \left|\frac{\alpha_L}{\eta_i^2 F_{k,l}^2\sin^2\phi_l}\cdot\left(\frac{\partial^2\eta}{\partial\theta^2}\right)_{i,k,l} + \frac{\alpha_L}{\eta_i^2 F_{k,l}^2}\left(\frac{\partial^2\eta}{\partial\phi^2}\right)_{i,k,l}\right.$$
$$- \frac{U\sin\theta_k}{\eta_i F_{k,l}\sin\phi_l}\left(\frac{\partial\eta}{\partial\theta}\right)_{i,k,l} + \left(\frac{\alpha_L\cot\phi_l}{\eta_i^2 F_{k,l}^2} + \frac{U\cos\phi_l\cos\theta_k}{\eta_i F_{k,l}}\right)$$
$$\left.\cdot\left(\frac{\partial\eta}{\partial\phi}\right)_{i,k,l} + \frac{2\alpha_L}{\eta_i F_{k,l}^2} + \frac{U\sin\phi_l\cos\theta_k}{F_{k,l}} - \left(\frac{\partial\eta}{\partial t}\right)_{i,k,l}\right|\cdot\frac{1}{(\Delta\eta)}$$

$$+\frac{U\sin\theta_k}{\eta_i F_{k,l}\sin\phi_l\cdot(\Delta\theta)}+\left|\frac{\alpha_L\cot\phi_l}{\eta_i^2 F_{k,l}^2}+\frac{U\cos\phi_l\cos\theta_k}{\eta_i F_{k,l}}\right|$$

$$\left.\cdot\frac{1}{(\Delta\phi)}\right)^{-1}\text{ for }1\le i\le N_\eta,\ 1\le k\le N_\theta,\text{ and }1\le l\le N_\phi \quad [37]$$

$$\Delta t_S=\min\left(\left(\left(\frac{1}{(\xi_j(F_{k,l}-B_{k,l})+B_{k,l})^2\sin^2\phi_l}\left(\frac{\partial\xi}{\partial\theta}\right)^2_{j,k,l}\right.\right.\right.$$

$$\left.+\frac{1}{(\xi_j(F_{k,l}-B_{k,l})+B_{k,l})^2}\left(\frac{\partial\xi}{\partial\phi}\right)^2_{j,k,l}+\frac{1}{(F_{k,l}-B_{k,l})^2}\right)$$

$$\cdot\frac{2\alpha_S}{(\Delta\xi)^2}+\frac{2\alpha_S}{(\xi_j(F_{k,l}-B_{k,l})+B_{k,l})^2\sin^2\phi_l\cdot(\Delta\theta)^2}$$

$$+\frac{2\alpha_S}{(\xi_j(F_{k,l}-B_{k,l})+B_{k,l})^2\cdot(\Delta\phi)^2}$$

$$+\frac{4\alpha_S}{(\xi_j(F_{k,l}-B_{k,l})+B_{k,l})^2\sin^2\phi_l\cdot(\Delta\xi\Delta\theta)}\cdot\left|\left(\frac{\partial\xi}{\partial\theta}\right)_{j,k,l}\right|$$

$$+\frac{4\alpha_S}{(\xi_j(F_{k,l}-B_{k,l})+B_{k,l})^2\cdot(\Delta\xi\Delta\phi)}\cdot\left|\left(\frac{\partial\xi}{\partial\phi}\right)_{j,k,l}\right|$$

$$+\left|\frac{\alpha_S}{(\xi_j(F_{k,l}-B_{k,l})+B_{k,l})^2\sin^2\phi_l}\left(\frac{\partial^2\xi}{\partial\theta^2}\right)_{j,k,l}\right.$$

$$+\frac{\alpha_S}{(\xi_j(F_{k,l}-B_{k,l})+B_{k,l})^2}\left(\frac{\partial^2\xi}{\partial\phi^2}\right)_{j,k,l} \quad [38]$$

$$-\frac{U\sin\theta_k}{(\xi_j(F_{k,l}-B_{k,l})+B_{k,l})\sin\phi_l}\left(\frac{\partial\xi}{\partial\theta}\right)_{j,k,l}$$

$$+\left(\frac{\alpha_S\cot\phi_l}{(\xi_j(F_{k,l}-B_{k,l})+B_{k,l})^2}+\frac{U\cos\phi_l\cos\theta_k}{\xi_j(F_{k,l}-B_{k,l})+B_{k,l}}\right)$$

$$\cdot\left(\frac{\partial\xi}{\partial\phi}\right)_{j,k,l}+\frac{2\alpha_S}{(F_{k,l}-B_{k,l})\cdot(\xi_j(F_{k,l}-B_{k,l})+B_{k,l})}$$

$$\left.+\frac{U\sin\phi_l\cos\theta_k}{F_{k,l}-B_{k,l}}-\left(\frac{\partial\xi}{\partial t}\right)_{j,k,l}\right|\cdot\frac{1}{(\Delta\xi)}$$

$$+\frac{U\sin\theta_k}{(\xi_j(F_{k,l}-B_{k,l})+B_{k,l})\sin\phi_l\cdot(\Delta\theta)}$$

$$+\left|\frac{\alpha_S\cot\phi_l}{(\xi_j(F_{k,l}-B_{k,l})+B_{k,l})^2}+\frac{U\cos\phi_l\cos\theta_k}{\xi_j(F_{k,l}-B_{k,l})+B_{k,l}}\right|$$

$$\left.\cdot\frac{1}{(\Delta\phi)}\right)^{-1}\quad\text{for}\quad 1\le j\le N_\xi,\ 1\le k\le N_\theta,\text{ and }1\le l\le N_\phi$$

and

$$\Delta t_F=\min\left(\left|\frac{2}{L}\left(-\frac{K_L}{F_{k,l}}\left(\frac{\partial T_L}{\partial\eta}\right)_{\eta=1}\right)_{k,l}+\frac{K_S}{F_{k,l}-B_{k,l}}\left(\frac{\partial T_S}{\partial\xi}\right)_{\xi=1}\right)_{k,l}\right|$$

$$\cdot\left(\frac{1}{F_{k,l}^2\sin^2\phi_l\cdot(\Delta\theta)^2}+\frac{1}{F_{k,l}^2(\Delta\phi)^2}\right) \quad [39]$$

$$+\frac{U\sin\theta_k}{F_{k,l}\sin\phi_l\cdot(\Delta\theta)}+\left|\frac{U\cos\phi_l\cos\theta_k}{F_{k,l}}\right|\cdot\left.\frac{1}{(\Delta\phi)}\right)^{-1}$$

$$\text{for}\quad 1\le k\le N_\theta\quad\text{and}\quad 1\le l\le N_\phi$$

where the minimums are with respect to every corresponding nodal point.

Table I. Thermophysical Data for Al-32. 7 Wt Pct Cu Eutectic Alloy

Eutectic temperature	821 K	Ref. 19
Vaporization temperature	2750 K*	Ref. 20
Latent heat	1.23×10^9 J/m^3	Ref. 21
Thermal conductivity in solid	118 W/m/K**	Ref. 22
Thermal conductivity in liquid	58.1 W/m/K	Ref. 22
Thermal diffusivity in solid	4.48×10^{-5} m^2/s	†
Thermal diffusivity in liquid	2.03×10^{-5} m^2/s	‡
Surface absorptivity on solid	0.035**	Ref. 23
Surface absorptivity on liquid	0.085	Ref. 23

*Vaporization temperature of pure aluminum as a substitute.

**Averaged from 293 K to eutectic temperature.

†Calculated using thermal conductivity in solid and specific heat of solid averaged from 293 K to eutectic temperature.[13]

‡Calculated using thermal conductivity in liquid and specific heat of liquid.[13]

Table II. Laser Processing Conditions

Laser power	1250 W*
Beam radius	120 μm
Beam travel velocity	0.2 to 2.0 m/s
Initial temperature of the substrate	293 K
Ambient temperature	293 K
Surface heat transfer coefficient	100 W/m^2/K
Protective gas	He

*Measured value quoted form Refs. 13 and 23 is used, because the value described in Ref. 2, 1500 W,, is nominal.

III. CALCULATED RESULTS AND DISCUSSION

Calculations were performed using the thermophysical properties of an Al-32.7 wt pct Cu eutectic alloy and processing conditions, as listed in Tables I and II. This binary eutectic alloy was chosen as a model system by virtue of the following reasons:

(1) the thermophysical data are well defined;
(2) the absorptivity, which controls the energy input in the substrate, has been measured;[23]
(3) the scale of the eutectic microstructure has been studied extensively in connection with the growth rate;[2] and
(4) the high thermal conductivity of aluminum alloys reduces the effects of fluid flow within the molten pool, which are not considered in the present simulation.

The processing conditions listed in Table II were set identical to those of the experiments performed by Zimmermann *et al.*, [2] which were compared with the calculated results. The temperature at the outer boundary of the heat-affected region was set to 303 K, because a further reduction in the temperature did not affect the calculated results significantly.

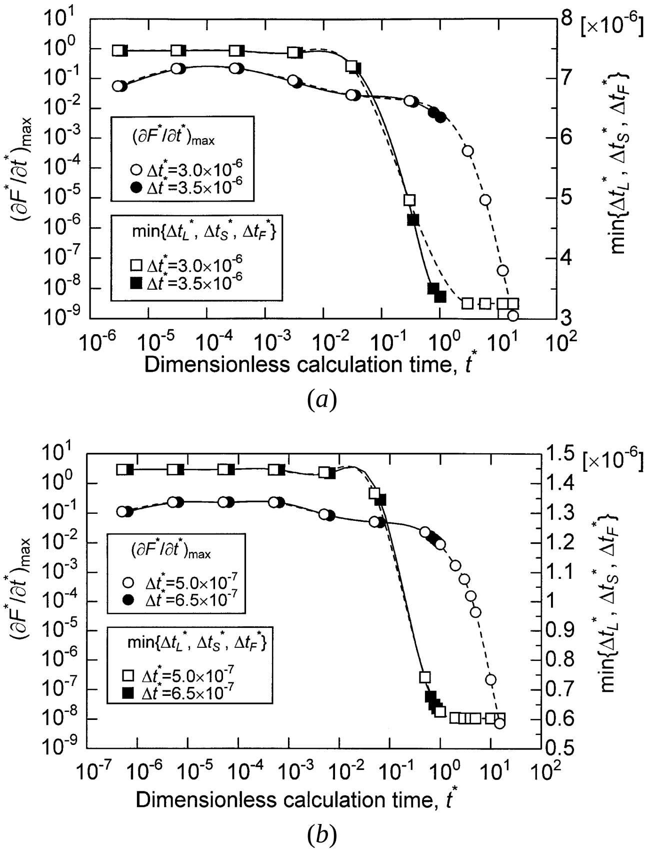

Fig. 3—Variations of maximum value of $\partial F^*/\partial t^*$, $(\partial F^*/\partial t^*)_{\max}$, and minimum value between Δt_L^*, Δt_S^*, and Δt_F^*, min $\{\Delta t_L^*, \Delta t_S^*, \Delta t_F^*\}$, with dimensionless calculation time t^* for a beam travel velocity of 0.6 m/s: (*a*) $N_\eta = 10$, $N_\xi = 40$, $N_\theta = 13$, and $N_\phi = 8$; and (*b*) $N_\eta = 10$, $N_\xi = 40$, $N_\theta = 19$, and $N_\phi = 12$.

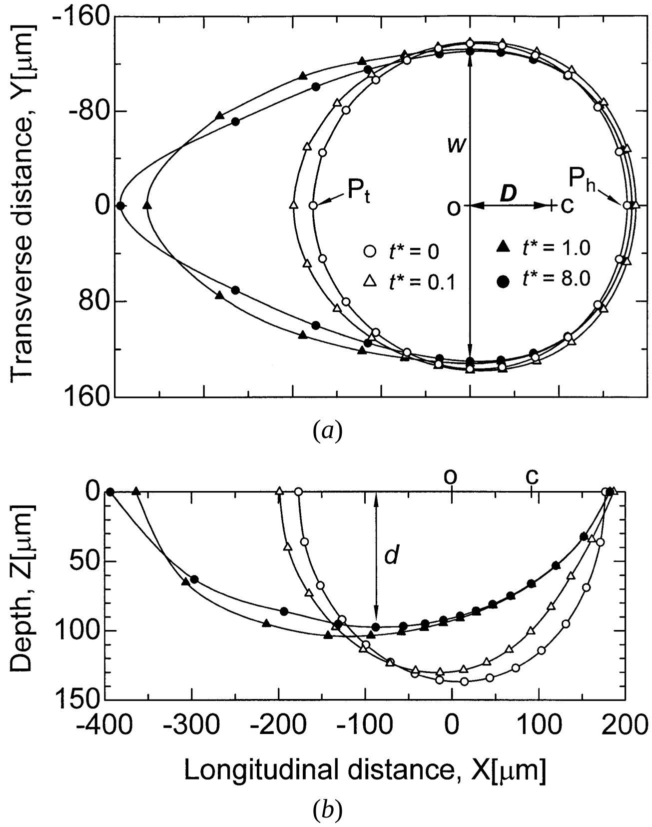

Fig. 4—Evolution of the molten pool with the lapse of calculation time for a beam travel velocity of 0.6 m/s.

A. *Steady-State Molten Pool*

In order for the steady-state molten pool to be obtained by the numerical simulation, a time step for calculation must satisfy Eq. [36]. Figure 3 is an example of the calculated results for $U = 0.6$ m/s, showing the variations of the maximum value of $\partial F^*/\partial t^*$, $(\partial F^*/\partial t^*)_{\max}$, and the minimum value between Δt_L^*, Δt_S^*, and Δt_F^*, min $(\Delta t_L^*, \Delta t_S^*, \Delta t_F^*)$, with the lapse of the dimensionless calculation time (t^*). Figure 3(a) shows a case where the numbers of nodal points are chosen as $N_\eta = 10$, $N_\xi = 40$, $N_\theta = 13$, and $N_\phi = 8$. When the dimensionless time step for calculation (Δt^*) is set to $3 \cdot 10^{-6}$, the value of min $(\Delta t_L^*, \Delta t_S^*, \Delta t_F^*)$ converges to $3.253276 \cdot 10^{-6}$, accompanying a sharp decrease in the maximum value of $\partial F^*/\partial t^*$ as the dimensionless calculation time becomes sufficiently long. When the dimensionless time step for calculation is, however, set to $3.5 \cdot 10^{-6}$, the value of min $(\Delta t_L^*, \Delta t_S^*, \Delta t_F^*)$ becomes less than $3.5 \cdot 10^{-6}$ after the dimensionless calculation time of 0.7745, with a failure of Eq. [36]. Therefore, the calculation becomes impossible after the dimensionless calculation time of 1.0206, due to a numerical instability. Similar findings are obtained for another case, where the numbers of nodal points are chosen as $N_\eta = 10$, $N_\xi = 40$, $N_\theta = 19$, and $N_\phi = 12$, as shown in Figure 3(b). These results demonstrate the validity of the stability condition given by Eq. [36] for determining a time step for calculation with respect to chosen spatial increments.

Figure 4 is an example of the calculated results for $U =$ 0.6 m/s, showing how the steady-state molten pool without undulation in shape is obtained with the lapse of the dimensionless calculation time from $t^* = 0$ to 8.0. In this calculation, the dimensionless time step was set to 10^{-6}. Thus, $t^* = 8.0$ corresponds to 8,000,000 time steps of calculation, at which the steady state is reached. Figure 4(a) shows the top views ($z = 0$ plane) of the molten pools at the various dimensionless times. Figure 4(b) shows the side views of the central longitudinal section ($y = 0$ plane) of the molten pools. In Figures 4(a) and (b), the discrete points with the same symbols represent the calculated solid-liquid interface positions at the corresponding times. The solid curves connecting the discrete points with the same symbols were drawn by interpolation using B-spline curves.

The molten pool at $t^* = 0$ is derived from the analytical solution of the Rosenthal moving-point source model, in which the latent heat due to melting and solidification is not considered. This solution was additionally used for determining the distance between the origin and the center of the laser beam. The origin was set so that the middle point of P_t and P_h, denoted in Figure 4(a), coincided with the origin. Thereby, the distance between the origin and the center of the laser beam was straightforwardly determined as 94 μm for this case.

The effect of the latent heat on the shape of the molten pool becomes evident on comparing the molten pools at $t^* = 0$, without consideration of the latent heat, and at 8.0, with consideration of the latent heat. The latent heat is absorbed at the front of the molten pool due to melting, while the latent heat is liberated at the tail of the molten pool due to solidification. This characteristic of the latent

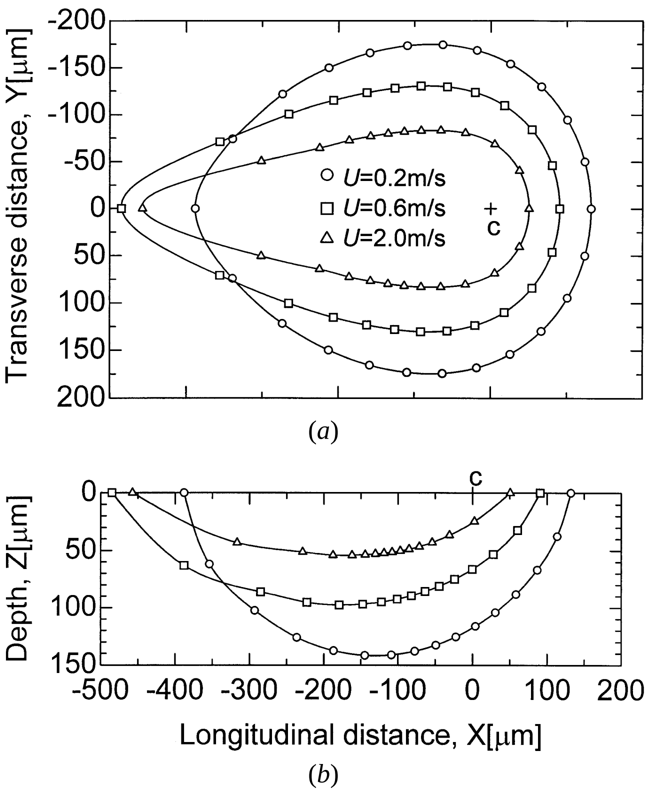

Fig. 5—Effect of beam travel velocity on the shape and size of the steady-state molten pool: (*a*) top view, $z = 0$ plane, and (*b*) side view, $y = 0$ plane, of the central longitudinal section of the molten pool.

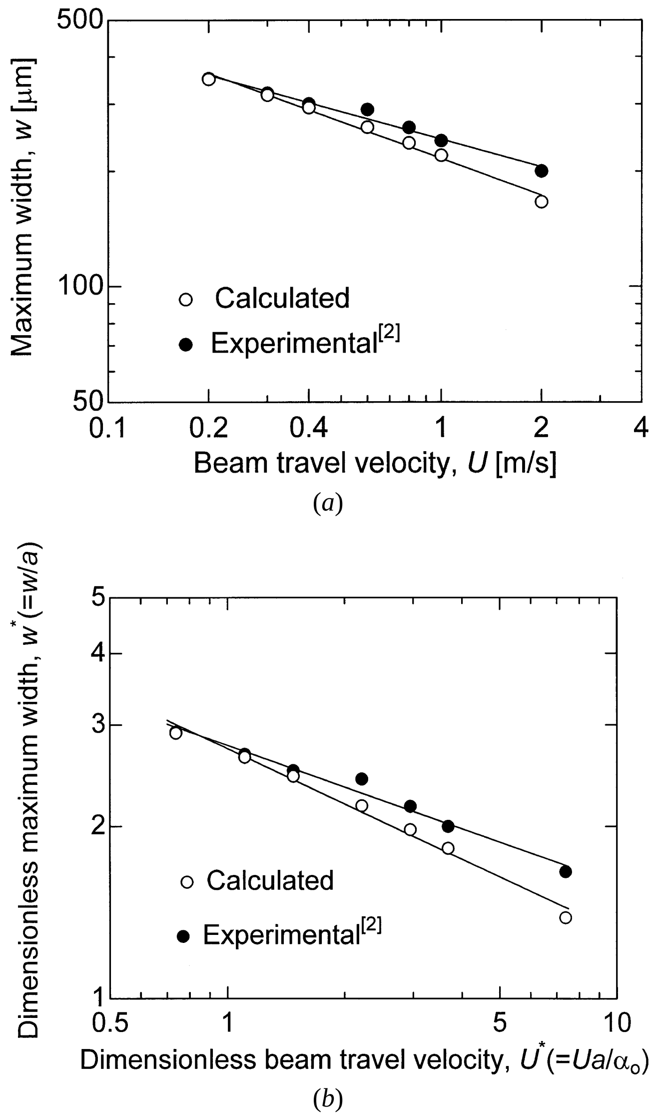

Fig. 6—Variation of maximum width of molten pool with beam travel velocity: (*a*) dimensional and (*b*) dimensionless.

heat affects the shape of the molten pool through the heat balance at the solid-liquid interface expressed in Eqs. [33] and [34]. Therefore, with the change in time from $t^* = 0$ to 8.0, the front of the molten pool moves toward the center of the laser beam and the tail of the molten pool moves away from the center of the laser beam, as shown in Figure 4(b). The maximum width of the molten pool at $t^* = 8.0$, denoted by w in Figure 4(a), does not change considerably from that of the molten pool at $t^* = 0$, as shown in Figure 4(a). However, the maximum depth of the molten pool at $t^* = 8.0$, denoted by d in Figure 4(b), is 40 μm smaller than that of the molten pool at $t^* = 0$, as shown in Figure 4(b). This result indicates that the consideration of the latent heat is important for the analysis of the laser surface-melting process to assess the molten-pool depth.

B. *Effect of the Beam Travel Velocity*

As shown in Figure 5, the change in beam travel velocity affects the steady-state shape and size of the molten pool, because it influences the irradiation time, defined by $2a/U$,[24] and advective heat transport in the negative x-direction. In this figure, the origin is set at the center of the laser beam, denoted by the letter C. The higher velocity of the laser beam causes a smaller molten pool and greater extension at the tail of the molten pool.

Figures 6 and 7 show the variations of calculated molten-pool dimensions with beam travel velocity. For comparison with the calculated results, experimental data obtained by Zimmermann *et al.*[2] are also presented in these figures. Although the present calculation neglects the convective heat transfer in the molten pool, the calculated results agree approximately with the experimental data.

The relationships between the maximum width of the molten pool (w(μm)) and the beam travel velocity (U(m/s)) are $w = 242.4U^{-0.2401}$ ($w^* = 2.763(U^*)^{-0.2401}$ in dimensionless terms) for the experimental data and $w = 215.9U^{-0.3189}$ ($w^* = 2.727(U^*)^{-0.3189}$ in dimensionless terms) for the calculated results.

The relationships between the maximum depth of the molten pool (d(μm)) and the beam travel velocity (U(m/s)) are $d = 68.12U^{-0.4296}$ ($d^* = 0.9943(U^*)^{-0.4296}$ in dimensionless terms) for the experimental data and $d = 76.08U^{-0.4148}$ ($d^* = 1.089(U^*)^{-0.4148}$ in dimensionless terms) for the calculated results.

This fact suggests that the convective heat transfer in the molten pool is of minor importance to the molten-pool size, within the range of processing conditions considered in the present study.

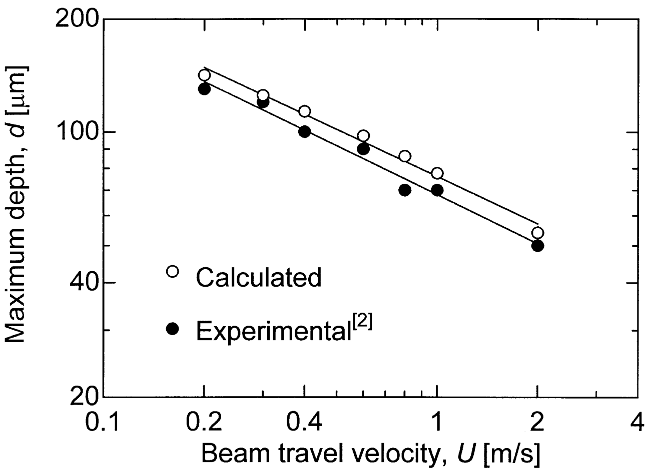

(*a*)

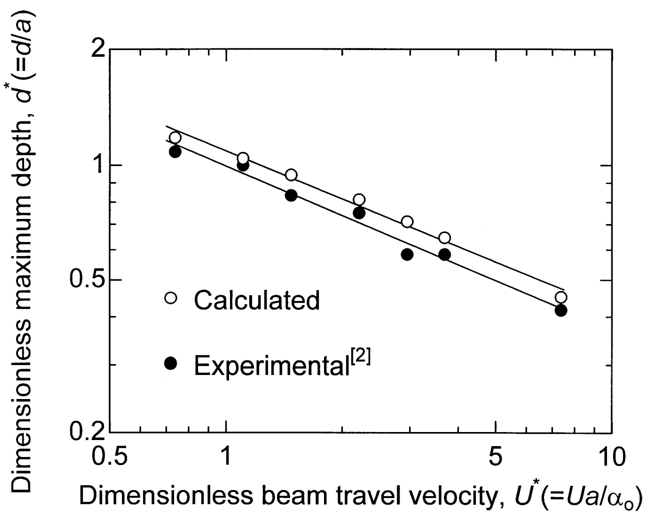

(*b*)

Fig. 7—Variation of maximum depth of molten pool with beam travel velocity: (*a*) dimensional and (*b*) dimensionless.

C. *Microstructure of the Laser Trace*

In the laser surface-melting process, the local solidification rate can be determined quantitatively from the shape of the molten pool.[2] Figure 8 is a schematic drawing of the central longitudinal section of the molten pool and the laser trace, showing the geometrical relationship between the beam travel velocity and the local solidification rate. The orientation of the solidifying microstructure tends to be perpendicular to the local solid-liquid interface. Thus, the local solidification rate is geometrically described as

$$V_S = U \cos \psi \qquad [40]$$

By expressing the curved-line segment (P_1P_2) of the solidification front as $z = g(x)$, the angle ψ is given by

$$\psi = \frac{\pi}{2} - \arctan\left(\frac{dg}{dx}\right) \qquad [41]$$

A combination of Eqs. [36] and [37] leads to the following equation:

$$V_S = U \sin\left(\arctan\left(\frac{dg}{dx}\right)\right) \qquad [42]$$

This equation demonstrates that the local solidification rate can be determined from the shape of the molten pool.

For the Al-32.7 wt pct Cu eutectic alloy, the microstructure consists of parallel lamellae at solidification rates of below 0.2 m/s,[2] and the experimental values of the interlamellar spacing (λ) and solidification rate follow the relationship[2] given by

$$\lambda^2 V_S = 88\ \mu\text{m}^3/\text{s} \qquad [43]$$

Substitution of Eq. [39] for V_S in Eq. [38] provides the equation describing the depth dependence of the interlamellar spacing.

Figure 9 shows the predicted and experimental[2] interlamellar spacing within the central longitudinal section of the laser trace, as a function of the height from the bottom of the laser trace. In this figure, the predicted interlamellar spacing is obtained through the aforementioned procedures

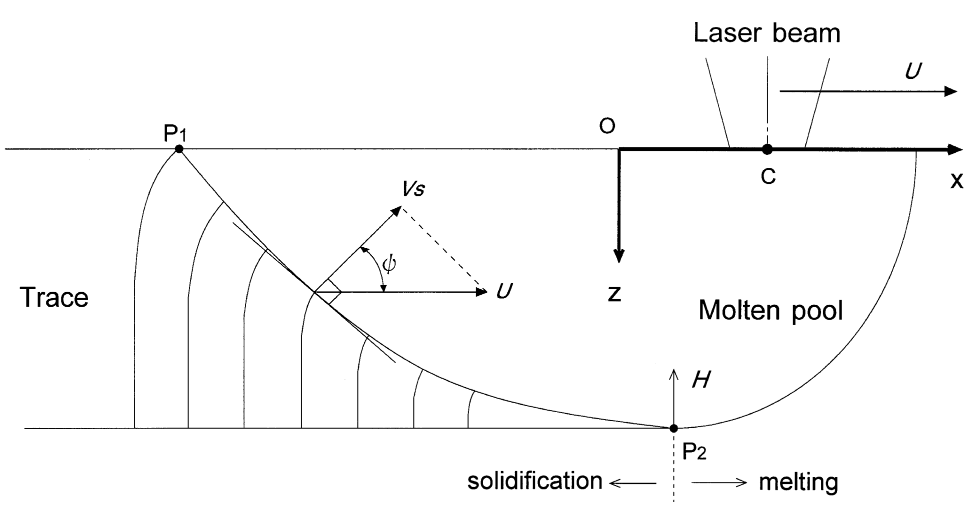

Fig. 8—Schematic drawing of the central longitudinal section of the molten pool and resultant laser trace.

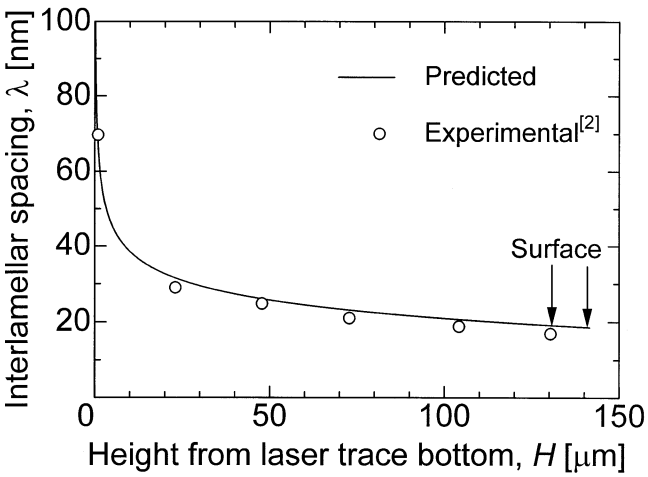

Fig. 9—Comparison between the predicted and experimental interlamellar spacing within the central longitudinal section of the laser trace for a beam travel velocity of 0.2 m/s.

using the calculated result for $U = 0.2$ m/s. This figure demonstrates that the predicted interlamellar spacing agrees well with the experimental data. Furthermore, it is worth noting that in this laser trace, most of the depth of the substrate has a fine microstructure with an interlamellar spacing of less than 30 nm. From these results, the numerical simulation presented in this study appears to be effective for a microscopic prediction as well as a macroscopic one.

IV. CONCLUSIONS

The formation of the steady-state molten pool during the laser surface-melting process was numerically simulated by applying the boundary-fixing method to a transient three-dimensional heat-conduction problem with a moving planar solid-liquid interface. Results obtained from the present calculations are as follows.

1. When the steady state is reached, the resulting molten pool is obtained without undulation in shape.
2. For an Al-32.7 wt pct Cu eutectic alloy substrate, the calculated molten-pool dimensions and the interlamellar spacing predicted using the calculated results agree approximately with experimental data.

NOMENCLATURE

a	beam radius (defined as the radial distance at which the power density falls to $1/e$ of the central value) (m)
$B(\theta, \phi)$	shape function of the outer boundary within the heat-affected region (m)
d	maximum depth of the molten pool (m)
D	distance between the origin of the spherical coordinate system and the center of the laser beam (m)
$F(\theta, \phi, t)$	shape function of the solid-liquid interface (m)
$g(x)$	shape function of the solidification front (m)
h	surface heat-transfer coefficient (W/m^2/K)
H	height from the bottom of the laser trace (m)
K	thermal conductivity (W/m/K)
L	latent heat (J/m^3)
N_η	number of nodal points in the η direction
N_ξ	number of nodal points in the ξ direction
N_θ	number of nodal points in the θ direction
N_ϕ	number of nodal points in the ϕ direction
P	total incident power in the laser beam (W)
q	power-density distribution in the laser beam (W/m^2)
r	radial coordinate (m)
t	time (s)
T	temperature (K)
T_a	ambient temperature (K)
T_B	temperature on the outer boundary of the heat-affected region (K)
T_{eu}	eutectic temperature (K)
T_f	temperature at the solid-liquid interface, equal to T_{eu} (K)
T_i	initial temperature of the substrate (K)
T_V	vaporization temperature (K)
U	beam travel velocity (m/s)
V_s	local solidification rate (m/s)
w	maximum width of the molten pool (m)
x, y, and z	spatial coordinates (m)

Greek Symbols

α	thermal diffusivity (m^2/s)
β	surface absorptivity (—)
Δt	time step for calculation (s)
Δt_F	time step defined by Eq. [39] (s)
Δt_L	time step defined by Eq. [37] (s)
Δt_S	time step defined by Eq. [38] (s)
$\Delta\eta$	spatial increment in the η direction, equal to $1/N_\eta$ (—)
$\Delta\xi$	spatial increment in the ξ direction, equal to $1/N_\xi$ (—)
$\Delta\theta$	spatial increment in the θ direction, equal to $\pi/(N_\theta - 1)$ (radians)
$\Delta\phi$	spatial increment in the ϕ direction, equal to $\pi/(2N_\phi - 1)$ (radians)
ε	surface emissivity, equal to $1 - \beta$, (—)
η	independent variable (Eq. [13]) (—)
θ	angle in spherical coordinate (radians)
θ_o	reference angle, equal to π (radians)
λ	interlamellar spacing (m)
ξ	independent variable (Eq. [14]) (—)
σ	Stefan–Boltzmann constant, equal to $5.67 \cdot 10^{-8}$ (W/m^2/K^4)
ϕ	angle in spherical coordinate (radians)
ϕ_o	reference angle equal to $\pi/2$ (radians)
ψ	angle between the vectors V_S and U (radians)

Subscripts and Superscripts

L	liquid region
S	solid region
O	reference quantity, average of those of the liquid and solid regions
*	dimensionless quantity
i, j, k, and l	nodal-point indices in the η, ξ, θ, and ϕ directions, respectively

REFERENCES

1. W.M. Steen: *Laser Material Processing*, Springer-Verlag, London, 1994, pp. 187-92.
2. M. Zimmermann, M. Carrard, and W. Kurz: *Acta Metall.*, 1989, vol. 37, pp. 3305-13.
3. Y. Nakano, K. Nishimoto, W.P. Zhang, and Y. Tamura: *Q. J. JWS*, 1991, vol. 9, pp. 122-28 (in Japanese).
4. W. Kurz and R. Trivedi: *Mater. Sci. Eng.*, 1994, vols. A179–A180, pp. 46-51.
5. W. Kurz, B. Giovanola, and R. Trivedi: *Acta Metall.*, 1986, vol. 34, pp. 823-30.
6. D.C. Baxter: *J. Heat Transfer, Trans. ASME*, 1962, vol. 84, pp. 317-26.
7. K. Katayama and M. Hattori: *Trans. Jpn. Soc. Mech. Eng.*, 1974, vol. 40, pp. 1404-11.
8. N. Shamsundar and E.M. Sparrow: *J. Heat Transfer, Trans. ASME*, 1975, vol. 97, pp. 333-40.
9. A.B. Crowley: *Int. J. Heat Mass Transfer*, 1978, vol. 21, pp. 215-19.
10. M. Paolini, G. Sacchi, and C. Verdi: *Int. J. Numer. Meth. Eng.*, 1988, vol. 26, pp. 1989-2007.
11. S. Kou, S. Hsu, and R. Mehrabian: *Metall. Trans. B*, 1981, vol. 12B, pp. 33-45.
12. K.V. Rama Rao and J.A. Sekhar: *Acta Metall.*, 1987, vol. 35, pp. 81-87.
13. A.F.A. Hoadley, M. Rappaz, and M. Zimmermann: *Metall. Trans. B*, 1991, vol. 22B, pp. 101-09.
14. J.L. Duda, F.M. Michael, H.N. Robert, and J.S. Vrentas: *Int. J. Heat Mass Transfer*, 1975, vol. 18, pp. 901-10.
15. T. Saitoh: *J. Heat Transfer, Trans. ASME*, 1978, vol. 100, pp. 294-99.
16. D. Rosenthal: *Trans. ASME*, 1946, vol. 68, pp. 849-66.
17. C.F. Gerald and P.O. Wheatley: *Applied Numerical Analysis*, Addison-Wesley Longman, Reading, MA, (1991), pp. 455-59.
18. P.J. Roache: *Computational Fluid Dynamics*, Hermosa Pub. Inc., Albuquerque, NM, 1976, p. 97 (Japanese translation).
19. T.B. Massalski: *Binary Alloy Phase Diagrams*, ASM, Metals Park, OH, 1986, vol. 1, pp. 103-08.
20. L.F. Mondolfo: *Aluminum Alloys: Structure and Properties*, 1st ed., Butterworth and Co., London, 1976, p. 56.
21. M.H. Burden and H. Jones: *J. Inst. Met.*, 1970, vol. 98, pp. 249-52.
22. M. Gündüz and J.D. Hunt: *Acta Metall.*, 1985, vol. 33, pp. 1651-72.
23. A. Frenk, A.F.A. Hoadley, and J.-D. Wagnière: *Metall. Trans. B*, 1991, vol. 22B, pp. 139-41.
24. A.M. Prokhorov, V.I. Konov, I. Ursu, and I.N. Mihăilescu: *Laser Heating of Metals*, Adam Hilger, Bristol, 1990, p. 209.